IOP Publishing Superconductor Science and Technology
Supercond. Sci. Technol. **27** (2014) 035004 (6pp) doi:10.1088/0953-2048/27/3/035004

Superconductivity in non-centrosymmetric $ThCoC_2$

T Grant[1], A J S Machado[2], D J Kim[1] and Z Fisk[1]

[1] Department of Physics and Astronomy, University of California-Irvine, Irvine, CA 92697, USA
[2] Escola de Engenharia de Lorena, Universidade de Sao Paulo, PO Box 116, Lorena, SP, Brazil

E-mail: tgrant@uci.edu

Received 24 August 2013, revised 10 December 2013
Accepted for publication 18 December 2013
Published 21 January 2014

Abstract

Superconductivity in compounds whose crystal structure lacks inversion symmetry are known to display intriguing properties that deviate from conventional BCS superconducting behavior. Here we report magnetization, resistivity, and heat capacity measurements on polycrystalline samples of $ThCoC_2$, which has been reported to crystallize in the non-centrosymmetric $CeNiC_2$ prototype structure, and show clear evidence of bulk superconductivity in $ThCoC_2$ with a critical temperature of $T_c = 2.65$ K. From the specific heat data we find a Sommerfeld coefficient of $\gamma = 8.38$ mJ mol^{-1} K^{-2} and a Debye temperature of $\Theta_D = 449$ K. Interestingly the H_{c2} superconducting phase diagram displays positive curvature, and the specific heat at low temperature deviates from conventional exponential temperature dependence, which is suggestive of possible unconventional superconducting behavior in $ThCoC_2$, similar to that seen in the isostructural and isoelectronic non-centrosymmetric superconductor $LaNiC_2$.

Keywords: noncentrosymmetric superconductor, carbon-based superconductor, ternary metal carbide, cobalt-based superconductor

(Some figures may appear in colour only in the online journal)

1. Introduction

One of the highlights of Solid State Chemistry in recent decades has been the discovery of many types of ternary transition metal carbides that crystallize in different novel prototype structures and exhibit interesting magnetic and electrical properties. These compounds by definition are composed of carbon, a transition metal, and a highly electropositive multivalent metal such as a lanthanide (Ln), Sc, Y, or Th. The complete ionization of the electropositive metal to stable ions Ln^{3+}, Y^{3+}, or Th^{4+} leads to a negatively charged transition metal–carbon sub-network, which can be regarded as an organometallic net [1–3]. An important characteristic of these carbide compounds is the presence of single and/or multiple metal–carbon and carbon–carbon bonds. Compounds of particular interest in this paper are those that crystallize in the $CeNiC_2$ prototype structure, which is base centered orthorhombic space group $Amm2$ (No. 38) [4]. The structure is formed from the stacking of alternating two-dimensional (2D) NiC_2 and distorted hexagonal rare-earth-metal sheets, with the structure of $ThCoC_2$, shown in figure 1. This kind of prototype structure is selective in electron count with the transition metals limited to group VIII Fe, Co, and Ni atoms [5]. In these compounds the stoichiometric formula is given by $LnTC_2$, YTC_2, or $ThCoC_2$ (T = Fe, Ni, or Co) and interestingly have short bond lengths between adjacent carbon atoms in the range of 1.32–1.47 Å, which is suggestive of carbon–carbon double bonds in the organometallic net, as shown figure 1.

More than 30 compounds have been found to crystallize in the same $CeNiC_2$ prototype structure, particularly from a series of rare-earth (R) carbides $RNiC_2$ and $RCoC_2$ [6–13]. Neutron diffraction studies on these series (R = Pr, Nd, Tb, Dy, Ho, Er, and Tm) [8–13] found different magnetic order between the series, with $RCoC_2$ compounds generally becoming ferromagnets and $RNiC_2$ compounds ordering antiferromagnetically in different spin configurations [13]. The studies found that the magnetic order arises from the 4f electrons confined on the rare earth sites, whereas the Co and Ni sites remain non-magnetic, and is also evident by a very weak temperature-dependent magnetic susceptibility in $YCoC_2$ [8], $YNiC_2$ [7], and $LaNiC_2$ [14].

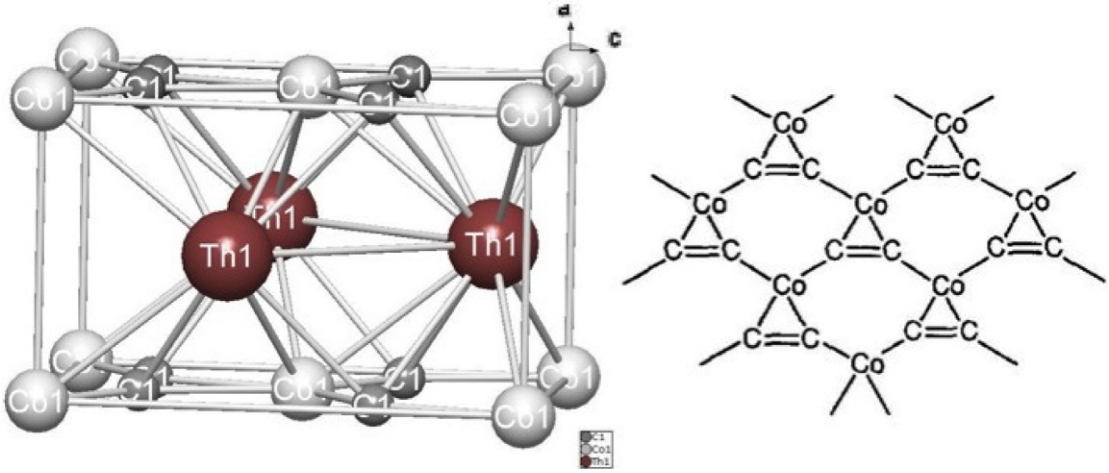

Figure 1. Left: crystal structure of $ThCoC_2$ in a $CeNiC_2$ prototype structure. Right: schematic representation of the anionic organometallic net for compounds that crystallize in the $CeNiC_2$ prototype structure, adapted from [1].

Interestingly $LaNiC_2$ becomes superconducting below 2.7 K [14] and is therefore classified as a non-centrosymmetric (NCS) superconductor since the $CeNiC_2$ prototype structure lacks an inversion center. This structural characteristic brings important implications for the physics in a superconducting state. Most superconducting materials possess an inversion center in their structures and have the Cooper pairs classified as either an even-parity spin-singlet, or an odd-parity spin-triplet state in accordance to the Pauli exclusion principle and parity conservation. However, the classification of the Cooper pairs into even or odd-parity states relies on the presence of an inversion center in the crystal structure. The absence of inversion symmetry introduces an antisymmetric spin–orbit coupling (ASOC) that lifts the spin degeneracy with spin-split Fermi surfaces, and importantly allows a mixing of spin-singlet and spin-triplet pairing states into a so called mixed-parity pairing state. Exotic properties can therefore emerge in parity violated superconductors such as time reversal symmetry (TRS) breaking, nodal gap structure, and other unconventional behavior attributed to the lack of inversion symmetry [15–20]. Indeed, it was recently demonstrated that $LaNiC_2$ shows TRS breaking in muon spin relaxation (μSR) measurements [21], and evidence for nodal gap structure in magnetic penetration depth measurements [22]. Therefore, in this work we examine the compound $ThCoC_2$ that is reported to be iso-structural [23] and iso-electronic to $LaNiC_2$, and show that $ThCoC_2$ is likely a new non-centrosymmetric superconductor with a critical temperature of $T_c = 2.65$ K. The results extracted from specific heat, magnetization, and resistivity measurements suggest that the superconducting state is similar to that seen in $LaNiC_2$ and possibly unconventional in origin.

2. Experiment

The polycrystalline $ThCoC_2$ sample was synthesized by arc melting together the stoichiometric amounts of the elements Th (3N), Co (4N), and graphite C (5N) on a water cooled Cu hearth in an arc-furnace under UHP (6N) Argon atmosphere and using a Zr getter. The samples were flipped over and re-melted 5 times to ensure good homogeneity, with minimal resultant weight loss (<0.7%) from arc melting. The sample was subsequently wrapped in tantalum foil and sealed in a quartz tube under vacuum for annealing treatment at 1100 °C for 14 days to improve sample quality and remove any unreacted magnetic impurities. Powder x-ray diffraction (XRD) patterns were obtained using a Rigaku MultiFlex diffractometer equipped with a monochromator providing Cu Kα ($\lambda = 1.540\,56$ Å) radiation. The diffraction pattern analysis and phase identification were done using MDI Jade software. Magnetization measurements were performed down to $T = 1.8$ K using a commercial VSM-SQUID magnetometer by Quantum Design. Electrical resistivity and heat capacity measurements were obtained using a physical property measurement system (PPMS) also by Quantum Design. The specific heat of a sample piece polished flat (~17 mg) was measured in the temperature range of 0.45–20 K with a He^3 calorimeter using the relaxation method. The resistivity sample was polished into a flat block (2.6 mm × 0.8 mm × 0.25 mm), and fine platinum wires were spot-welded to the sample as voltage and current leads for the standard four-probe method. The AC resistivity was measured down to 0.6 K with an applied current of 10 mA using a Linear Research Inc. model LR700 AC resistance-bridge and controlled by Lab View data acquisition software.

3. Results and discussion

Figure 2 shows the XRD pattern and corresponding Miller indices for the annealed polycrystalline $ThCoC_2$ sample. The peaks are indexed to the orthorhombic $CeNiC_2$ prototype structure with space group $Amm2$ (38), and the refinement of the lattice parameters yields $a = 3.8053$ Å, $b = 4.5321$ Å, and $c = 6.1424$ Å, in good agreement with results reported in literature [23]. These results suggest that the $ThCoC_2$ sample is phase pure at least within the standard detection limit for powder XRD method (~5%), and is consistent with the $CeNiC_2$ prototype structure. To our knowledge the investigation of $ThCoC_2$ compound has been rather limited [23], and therefore

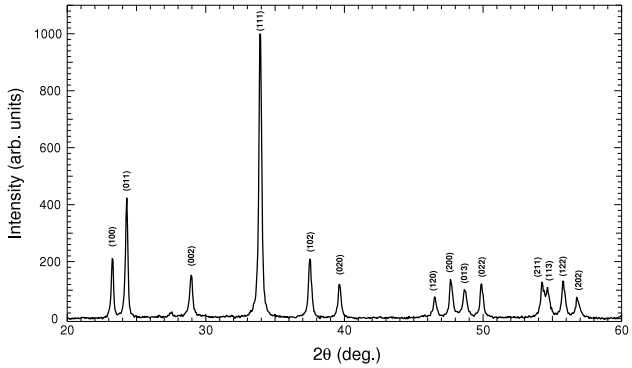

Figure 2. Room-temperature powder x-ray diffraction pattern for an annealed $ThCoC_2$ sample, along with corresponding Miller indices of the $CeNiC_2$ prototype structure.

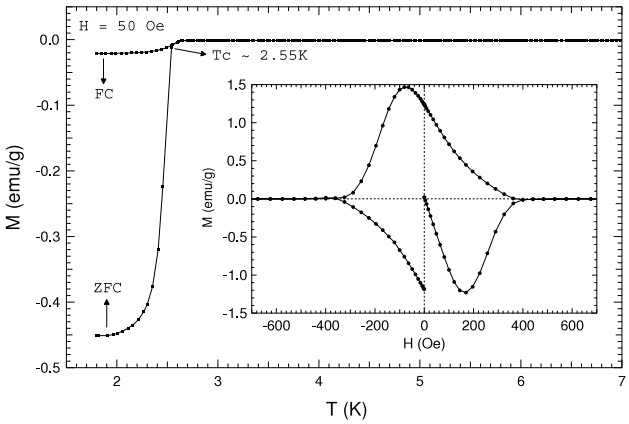

Figure 3. Temperature dependent magnetization in an applied magnetic field of $H = 50$ Oe, and displaying zero-field cooled (ZFC) and field cooled (FC) sweeps. Inset displays M versus H curve at $T = 1.8$ K.

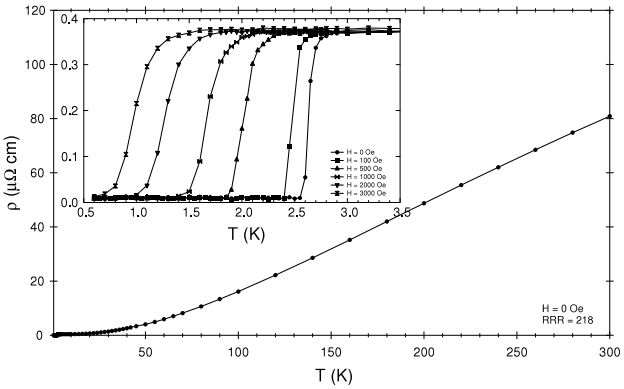

Figure 4. Electrical resistivity as a function of temperature between 0.6 and 300 K. Inset displays the superconducting transition in various applied magnetic fields.

it would be highly desirable to have additional in-depth structure determination by single crystal x-ray or neutron diffraction experiments to definitively demonstrate $ThCoC_2$ crystallizes in the non-centrosymmetric $CeNiC_2$ prototype structure, as has been shown for many of the other tertiary rare-earth carbides RTC_2 by neutron diffraction studies [8–13].

The temperature dependent magnetization using zero-field cooled (ZFC) and field cooled (FC) method using an applied 50 Oe magnetic field shows a clear diamagnetic transition onset around 2.55 K in figure 3. It should be noted that the as-cast samples slowly decomposed in air and had a small residual ferromagnetic signal, likely from small inclusions of unreacted Cobalt or a Cobalt binary, which makes the annealing treatment critical to stabilize the sample and eliminate any magnetic impurities. The hysteresis between ZFC and FC regimes indicate $ThCoC_2$ is a type II superconductor. Without correcting for demagnetization or sample size effects, we estimate the superconducting volume fraction (ZFC) to be 110% of perfect diamagnetism, which suggests possible bulk superconductivity. The Meissner flux expulsion (FC) is about 5% of the diamagnetic flux expulsion, a characteristic of strong flux pinning. The inset in figure 3 displays 4-quadrant M versus H data at $T = 1.8$ K and shows weak type II superconducting behavior.

Sample resistivity from 0.6–300 K is presented in figure 4, with the figure inset showing the superconducting transition suppressed with applied magnetic field. The polycrystalline $ThCoC_2$ sample is a very good metal with resistivity increasing linearly above $T > 100$ K at a rate of 0.33 $\mu\Omega$ cm K^{-1}, and an extremely low residual resistivity of 0.37 $\mu\Omega$ cm at $T = 4$ K. The resultant residual resistivity ratio (RRR $= \rho_{300}/\rho_4$) is thus a very large RRR $= 218$, indicating excellent alloy quality of the sample. The zero magnetic field data shows a sharp superconducting transition centered at $T_c = 2.65$ K and a zero-resistance temperature of $T_c = 2.55$ K. The sharp superconducting transition ($\Delta T_C \sim 0.2$ K) is consistent with the magnetization measurements and is also indicative of good sample quality.

While the magnetization and resistivity data suggest bulk superconductivity in $ThCoC_2$, an anomaly in the specific heat measurement is necessary for confirmation. Figure 5 displays the specific heat divided by temperature (C/T) versus T^2 in various applied magnetic fields. A jump in the specific heat is clearly observed with the midpoint of the transition at $T_c = 2.53$ K and a small transition interval $\Delta T_C \sim 0.3$ K . The consistency between the magnetization, resistivity, and heat capacity transitions is clear evidence of bulk superconductivity in $ThCoC_2$. The expected suppression of the superconducting transition with applied magnetic field is also seen in figure 5, along with a broadening of the transition that is not unusual for polycrystalline samples.

Analysis of the superconducting state first requires a comparison to the normal state specific heat C_n. The normal state specific heat is comprised of the electronic contribution C_e and the lattice contribution $C_{lattice}$, such that $C_n = C_e + C_{lattice}$. The electronic contribution is the linear Fermi liquid term $C_e = \gamma T$, with γ being the Sommerfeld coefficient. The lattice contribution to the heat capacity at low temperature is usually described just by the cubic Debye model term βT^3; however an increasing deviation above T_c requires the addition of the next higher order phonon dispersion term, such that $C_{lattice} = \beta T^3 + \delta T^5$. Fitting the normal state specific heat data to the expression $C_n = \gamma T + \beta T^3 + \delta T^5$ results in the fit parameters $\gamma = 8.38$ mJ mol^{-1} K^{-2}, $\beta = 0.0856$ mJ mol^{-1} K^{-4},

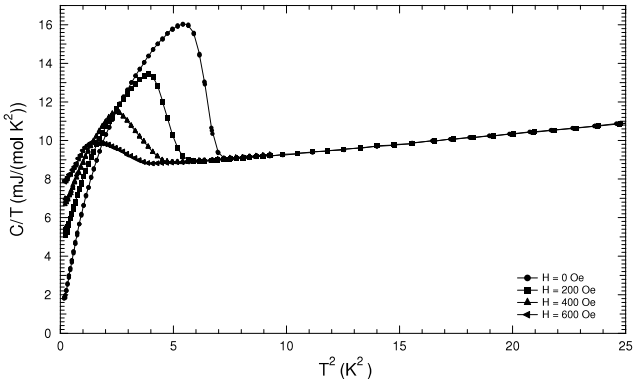

Figure 5. Specific heat divided by temperature (C/T) versus T^2 in various applied magnetic fields.

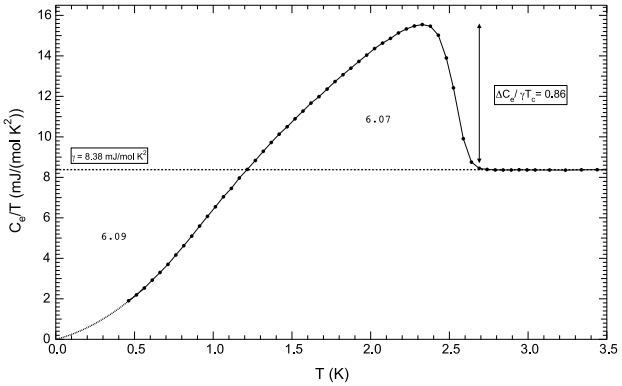

Figure 6. Temperature dependence of the electronic specific heat contribution divided by temperature (C_e/T). The calculated upper (6.07 mJ mol^{-1} K^{-1}) and lower (6.09 mJ mol^{-1} K^{-1}) area between the data and the value demonstrates entropy balance.

and $\delta = 5.59 \times 10^{-4}$ mJ mol^{-1} K^{-6}. The β value corresponds to a Debye temperature of $\Theta_D \sim 449$ K. The Sommerfeld coefficient γ suggests a low density of states at the Fermi level typical of other transition metal superconductors, with corresponding $LaNiC_2$ compound having $\gamma = 7.83$ mJ mol^{-1} K^{-2} and $\Theta_D \sim 496$ K for comparison [14].

Subtraction of the phonon contribution C_{lattice} from the total specific heat allows analysis of just the electronic contribution C_e, displayed here as C_e/T versus T in figure 6. The analysis of the specific heat anomaly shows the magnitude of the jump at T_c to be $\Delta C_e/\gamma_n T_c \sim 0.86$, which is significantly smaller than the weak-coupling BCS limit of 1.43. Since the superconducting transition is a second order phase transition, thermodynamics requires the entropies of the normal and superconducting states to be equal at the transition temperature T_c. This equality has the convenient geometric representation in figure 6 that the two enclosed areas above and below the $\gamma = 8.38$ mJ mol^{-1} K^{-2} baseline must be equal. The entropy balance is demonstrated in figure 6 with good agreement between the upper area of 6.07 mJ mol^{-1} K^{-1}, and lower area of 6.09 mJ mol^{-1} K^{-1} after the low temperature data is extrapolated to the origin. This thermodynamic consistency shows the lack of a residual heat capacity from impurity phases and demonstrates the excellent sample quality with full superconducting volume.

The microscopic theory of superconductivity predicts the electronic specific heat of conventional fully gapped s-wave superconductors to display a low-temperature exponential behavior of the form $\exp[-\Delta(0)/k_B T]$. The electronic specific heat for $ThCoC_2$ does not appear to follow this exponential temperature dependence that is expected for conventional BCS superconductors. This deviation from exponential behavior is visualized in figure 7, which displays the logarithmic graph of the electronic specific heat versus the inverse reduced temperature (T_c/T). Clearly the data shows a marked deviation at low temperature from a linear plot in figure 7 that would be expected for conventional superconductivity. Indeed it was shown that the specific heat of the analog $LaNiC_2$ compound also deviates from conventional exponential behavior with a low-temperature T^3 dependence [14] that is consistent with nodes in the energy gap, in addition to other evidence of non-conventional behavior of time reversal symmetry breaking in μSR measurements [21], and evidence for nodal gap structure with T^2 dependence in magnetic penetration depth measurements [22]. It is worth noting that earlier conflicting reports on $LaNiC_2$ conclude conventional BCS behavior in heat capacity [24] and Nuclear quadrupole resonance (NQR) measurements [25]; however the recent report by Bonalde *et al* [22] shows that is likely a result of the measurements sensitivity to magnetic Fe impurities introduced by lower quality Ni (3N) and the insufficient low temperature evaluation of the superconducting state in those studies. They correctly point out that temperatures below $0.3T_c$ are needed to properly determine the structure of the energy gap, in which they measured magnetic penetration depth down to $\sim 0.017T_c$ in $LaNiC_2$. The $ThCoC_2$ samples examined here are comparative to the higher quality $LaNiC_2$ samples, with the characteristic measurements indicating excellent $ThCoC_2$ sample quality without the signature of impurities being readily apparent. It is therefore not unreasonable to expect possible unconventional behavior for $ThCoC_2$ in future lower temperature examinations of the superconducting state.

The upper critical field H_{C2} as a function of temperature from the resistivity and specific heat data is plotted in figure 8, showing good agreement between the measurements. Unexpectedly the superconducting phase diagram has positive curvature instead of the conventional dome like plot separating the superconducting and normal state domains. Both the midpoint of the resistivity transition and the zero resistance values are plotted to emphasize this unusual behavior, showing positive curvature close to T_c then transitioning into an apparent linear behavior below $T < 1.4$ K. An accurate estimate of the upper critical field $H_{C2}(0)$ at absolute zero is difficult without conventional modeling, but it is evident that superconductivity in $ThCoC_2$ is quickly suppressed in magnetic field with H_{C2} only 3000 Oe at $T = 0.6$ K. Interestingly, examples of positive curvature in the upper critical field diagram include the borocarbides $LnNi_2B_2C$ [26, 27], magnesium diboride MgB_2 [28], the non-centrosymmetric $Li_2(Pd, Pt)_3B$ [29], and the non-centrosymmetric heavy-fermion superconductor $CeRhSi_3$ [30]. This kind of behavior can be attributed to interband coupling that can occur within a

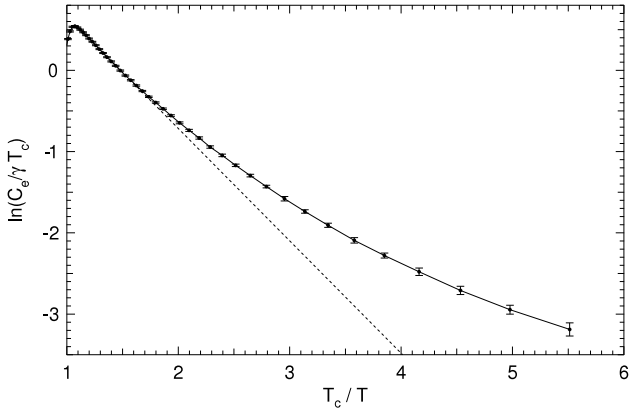

Figure 7. Logarithmic plot of the normalized electronic specific heat ($C_e/\gamma T_c$) versus inverse reduced temperature (T_c/T). The inserted dashed line represents the expected linear plot for a conventional BCS superconductor, emphasizing the deviation at low temperature.

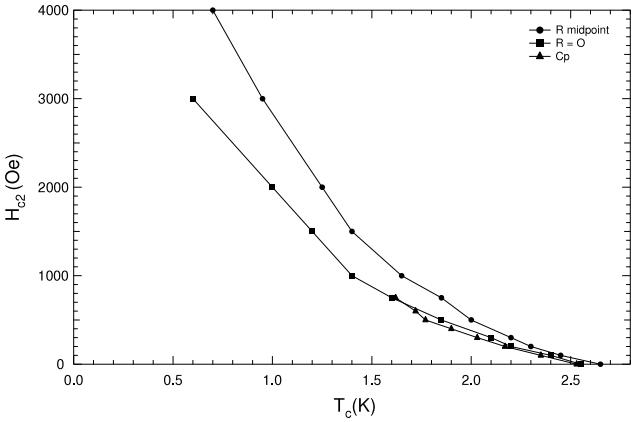

Figure 8. Temperature dependence of the upper critical field H_{c2} from resistivity (R) and specific heat (C_p) data, showing unusual positive curvature for the superconducting phase diagram.

multiband model [27, 31], with the small gap contributing at low temperature. In fact, a recent study on the superconducting state of $LaNiC_2$ also displays positive curvature near T_c and an enhancement of $H_{c2}(0)$ [31]. Chen *et al* systematically measured the low temperature London penetration depth, heat capacity, and resistivity, and argue the superconducting state in $LaNiC_2$ is best described by a two-gap BCS model, which is the likely result of a moderate value of the ASOC that splits the spin degenerate bands. Within this scenario the analog non-centrosymmetric superconductor $ThCoC_2$ could be a new example of a multiband compound, making additional low temperature characterizations of the superconducting state necessary to determine the exact nature of the energy gap.

4. Conclusion

In summary, polycrystalline samples of the reported non-centrosymmetric $ThCoC_2$ compound were characterized by magnetization, resistivity, and heat capacity measurements that unambiguously show bulk superconductivity with a critical temperature of $T_c = 2.65$ K. The superconducting state shows interesting behavior with a deviation from conventional BCS exponential temperature dependence in the specific heat, and positive curvature in the superconducting phase diagram. These results, in conjunction with those of analog non-centrosymmetric superconductor $LaNiC_2$, suggest possible unconventional superconducting behavior and warrant future low temperature investigations of the superconducting state in $ThCoC_2$. The limited reports on $ThCoC_2$ also make it a good candidate for precise structure analysis by such methods as single crystal x-ray or neutron diffraction experiments.

Acknowledgment

This work was graciously supported by the AFOSR-MURI.

References

[1] King R B 1994 *Russ. Chem. Bull.* **43** 1285
[2] King R B 1990 *Inorg. Chem.* **29** 2164
[3] Lee S, Jeitschko W Z and Hoffman R D 1989 *Inorg. Chem.* **28** 4094
[4] Bodak O I and Marusin E P 1979 *Dopov. Akad. Nauk Ukr. SSR Ser.* A **12** 1048
[5] Li J and Hoffmann R 1989 *Chem. Mater.* **1** 83
[6] Jeitschko W and Gerss M H 1986 *J. Less-Common Met.* **116** 147
[7] Kotsanidis P and Yakinthos J K 1989 *J. Less-Common Met.* **152** 287
[8] Schafer W, Will G, Kotsanidis P A and Yakinthos J K 1990 *J. Magn. Magn. Mater.* **83** 13
[9] Schafer W, Kockelmann W, Will G, Kotsanidis P A, Yakinthos J K and Linhart J 1994 *J. Magn. Magn. Mater.* **132** 243
[10] Yakinthos J K, Kotsanidis P A, Schafer W and Will G 1990 *J. Magn. Magn. Mater.* **89** 299
[11] Yakinthos J K, Kotsanidis P A, Schafer W, Kockelmann W, Will G and Reimers W 1994 *J. Magn. Magn. Mater.* **136** 327
[12] Schafer W, Will G, Yakinthos J K and Kotsanidis P A 1992 *J. Alloys Compounds* **180** 251
[13] Schafer W, Kockelmann W, Will G, Yakinthos J K and Kotsanidis P A 1997 *J. Alloys Compounds* **250** 565
[14] Lee W H, Zeng H K, Yao Y D and Chen Y Y 1996 *Physica* C **266** 138
[15] Bauer E, Hilscher G, Michor H, Paul C, Scheidt E W, Gribanov A, Seropegin Y, Noel H, Sigrist M and Rogl P 2004 *Phys. Rev. Lett.* **92** 027003
[16] Kimura N, Ito K, Aoki H, Uji S and Terashima T 2007 *Phys. Rev. Lett.* **98** 197001
[17] Yuan H Q, Agterberg D F, Hayashi N, Badica P, Vandervelde D, Dogano K, Sigrist M and Salamon M B 2006 *Phys. Rev. Lett.* **97** 017006
[18] Kim J S, Kremer R K, Jepsen O and Simon A 2006 *Curr. Appl. Phys.* **6** 897
[19] Klimezuk T, Ronning F, Sidorov V, Cava R J and Thompson J D 2007 *Phys. Rev. Lett.* **99** 257004
[20] Chen J B, Salamon M B, Akutagawa S, Akimitsu J, Singleton J, Zang J L, Jiao L and Yuan H Q 2011 *Phys. Rev.* B **83** 144529
[21] Hillier A D, Quintanilla J and Cywinski R 2009 *Phys. Rev. Lett.* **102** 117007
[22] Bonalde I, Ribeiro R L, Syu K J, Sung H H and Lee W H 2011 *New J. Phys.* **13** 123022
[23] Gerss M H and Jeitschko W 1986 *Mater. Res. Bull.* **21** 209

[24] Pecharsky V K, Miller L L and Gschneidner K A 1998 *Phys. Rev.* B **58** 497
[25] Iwamoto Y, Iwasaki Y, Ueda K and Kohara T 1998 *Phys. Lett.* A **250** 439
[26] Takagi H, Cava R J, Eisaki H, Lee J O, Mizuhashi K, Batlogg B, Uchida S, Krajewski J J and Peck W F 1994 *Physica* C **228** 389
[27] Shulga S V, Drechsler S L, Fuchs G, Muller K H, Winzer K, Heinecke M and Krug K 1998 *Phys. Rev. Lett.* **80** 1730
[28] Takano Y, Takeya H, Fujii H, Kumakura H, Hatano T and Togano K 2001 *Appl. Phys. Lett.* **78** 2914
[29] Peets D C, Eguchi G, Kriener M, Harada S, Shamsuzzamen Sk Md, Inada Y, Zheng G Q and Maeno Y 2011 *Phys. Rev.* B **84** 054521
[30] Kimura N, Ito K, Aoki H, Uji S and Terashima T 2007 *Phys. Rev. Lett.* **98** 197001
[31] Chen J, Jiao L, Zhang J L, Chen Y, Yang L, Nicklas M, Steglich F and Yuan H Q 2013 *New J. Phys.* **15** 053005